NeuroImage 219 (2020) 117029

Contents lists available at ScienceDirect

NeuroImage

journal homepage: www.elsevier.com/locate/neuroimage

Gradients of functional organization in posterior parietal cortex revealed by visual attention, visual short-term memory, and intrinsic functional connectivity

Ray W. Lefco, James A. Brissenden, Abigail L. Noyce, Sean M. Tobyne, David C. Somers *

Department of Psychological and Brain Sciences, Boston University, 64 Cummington Mall, Boston, MA, 02215, USA

ARTICLE INFO

Keywords:
Resting-state functional connectivity
Intraparietal sulcus
Multiple object tracking
Visual working memory
Retinotopy

ABSTRACT

Visual attention and visual working memory tasks recruit a common network of lateral frontal cortical (LFC) and posterior parietal cortical (PPC) regions. Here, we examine finer-scale organization of this frontoparietal network. Three LFC regions recruited by visual cognition tasks, superior precentral sulcus (sPCS), inferior precentral sulcus (iPCS), and mid inferior frontal sulcus (midIFS) exhibit differential patterns of resting-state functional connectivity to PPC. A broad dorsomedial to ventrolateral gradient is observed, with sPCS connectivity dominating in the dorsomedial PPC band, iPCS dominating in the middle band, and midIFS dominating in the ventrolateral band. These connectivity-defined subregions of PPC capture differential task activation between a pair of visual attention and working memory tasks. The relative functional connectivity of sPCS and iPCS also varies along the rostral-caudal axis of the retinotopic regions of PPC. iPCS connectivity is relatively stronger near the IPS0/IPS1 and IPS2/IPS3 borders, especially on the lateral portions of these borders, which each preferentially encode central visual field representations. In contrast, sPCS connectivity is relatively stronger elsewhere in retinotopic IPS regions which preferentially encode peripheral visual field representations. These findings reveal fine-scale gradients in functional connectivity within the frontoparietal visual network that capture a high-degree of specificity in PPC functional organization.

1. Introduction

Many visual cognition tasks drive activity within lateral frontal cortex (LFC) and posterior parietal cortex (PPC) (e.g., Hagler et al., 2006; Szczepanski et al., 2010; Ester et al., 2016). Functional and structural connectivity analyses (Mars et al., 2011; Power et al., 2011; Sallet et al., 2013; Cole et al., 2014; Brissenden et al., 2016) demonstrate that these frontal and parietal visual attention regions form a broad network. Task-based fMRI studies reveal functional subdivisions with frontal and parietal cortex. Visual attention tasks have commonly elicited frontal lobe activation near the intersection of the superior frontal sulcus and the superior branch of the precentral sulcus (sPCS) and the intersection of the inferior frontal sulcus and the inferior branch of the precentral sulcus (iPCS) (Hagler et al., 2006; Szczepanski et al., 2010; Michalka et al., 2015; Brissenden et al., 2016; Ester et al., 2016; Noyce et al., 2017). Visual tasks with stronger cognitive demands often produce more anterior cortical activity in the middle frontal gyrus and/or the midsection of inferior frontal sulcus (midIFS) (Hagler et al., 2006; Badre, Keyser & D'Esposito, 2010; Barch et al., 2013). Within PPC, retinotopic mapping studies reveal a swath of functional regions, including IPS0, IPS1, IPS2, IPS3, and IPS4 that each represent the contralateral visual hemifield (Silver et al., 2005; Swisher et al., 2007; Konen and Kastner, 2008). These maps tile the fundus and medial bank of the intraparietal sulcus and adjoining superior parietal lobule. Visual cognition task recruitment in PPC includes these regions and those abutting them (Szczepanski et al., 2010; Sheremata et al., 2010; Jerde et al., 2012; Bettencourt and Xu, 2016).

Intrinsic functional connectivity analysis identifies two primary visual attention subnetworks that each span frontal and parietal cortex: a dorsal attention network (DAN) that includes sPCS, iPCS, and the IPS visual maps, and a cognitive control network (CCN) that includes midIFS/middle frontal gyrus and the lateral bank of IPS (Power et al., 2011; Yeo et al., 2011). However, the finer-scale functional organization of these fronto-parietal networks remains debated (Mars et al., 2011; Sallet et al., 2013; Cole et al., 2014; Glasser et al., 2016). One promising approach is to examine intrinsic functional connectivity in individuals

* Corresponding author.
E-mail address: somers@bu.edu (D.C. Somers).

https://doi.org/10.1016/j.neuroimage.2020.117029
Received 17 October 2019; Received in revised form 27 April 2020; Accepted 4 June 2020
Available online 8 June 2020

(Braga and Buckner, 2017; Gordon et al., 2017); however, no consensus yet exists. Here, we examined whether patterns of heterogeneous functional connectivity between frontal and parietal cortex correspond to task-based and retinotopic landmarks within PPC.

To investigate finer-scale organization within the network of frontal and parietal visual attention regions, we performed individual-subject and group-level analyses of task and resting-state fMRI data. We first employed a visual working memory task to functionally identify three LFC regions, sPCS, iPCS, and midIFS, in each hemisphere of each individual. We then contrasted the patterns of resting-state functional connectivity from each of these ROIs to reveal group-level differences in their connectivity with PPC. Although each frontal region connected broadly within PPC, differential gradients in connectivity were evident. From these analyses we defined group-level regions of interest (ROIs) within frontal and parietal cortex. We then examined task activation in two attentionally demanding visual tasks that differed in their task demands: a change-detection visual working memory task (VWM-cd) and a multiple object tracking visual attention task (MOT). Although both tasks strongly drove activation in frontal and parietal cortex, contrasting the two tasks revealed differential patterns of recruitment in both cortical lobes. These task-based differences were consistent with the frontoparietal subnetworks revealed by the connectivity analysis. Group-level analysis further revealed an alternating pattern of waxing and waning of the relative connectivity strengths of sPCS and iPCS to retinotopic IPS. Connectivity with iPCS was relatively stronger at the areal borders between IPS0/IPS1, and IPS2/IPS3, most prominently at the lateral side of each border, whereas sPCS connectivity was stronger elsewhere within IPS. iPCS-dominant IPS subdomains corresponded with established representations of the central visual field, and sPCS-dominant connectivity with representations of the peripheral visual field (Swisher et al., 2007; Mackey et al., 2017). These findings suggest that functional differences between these frontal-parietal subnetworks may reflect differences between fovea-related and periphery-related processes in visual cognition.

2. Materials and methods

2.1. Subjects

20 subjects participated in this study. All studies were performed in accordance with the code of Ethics of the World Medical Association (Declaration of Helsinki). The Institutional Review Board of Boston University approved all experimental procedures, and all subjects received compensation and provided written informed consent to participate in the study. Subjects were recruited from Boston University and the greater Boston area. All subjects were healthy, right handed, and had normal or corrected-to-normal vision. Subjects participated in between one and three different fMRI studies. Study 1: Resting-state fMRI data were collected from 14 individuals (6 female). Visual vs. auditory working memory task fMRI results for these 14 subjects were previously reported (Noyce et al., 2017, 2018), and these findings were used to create regions of interest (ROIs) in lateral frontal cortex for the resting-state analysis described here. Study 2: Visual working memory change-detection (VWM-cd) task fMRI data were collected from 9 individuals (3 female). Study 3: Multiple object tracking (MOT) task fMRI data were collected from 9 individuals (5 female). 4 subjects participated in both MOT and VWM-cd experiments. Of the 14 resting-state subjects, 3 participated in both MOT and VWM-cd, 4 subjects participated in VWM-cd only, and 1 subject participated in MOT only.

2.2. MRI acquisition

All scanning data were collected at the Center for Brain Science Neuroimaging Facility at Harvard University (3T Siemens Trio TIM system equipped with a 32-channel matrix head coil.) A high-resolution (1.0 × 1.0 × 1.3 mm voxel size, TR = 6.6 ms, TE = 2.9 ms, flip angle = 8°) MP-RAGE sampling structural T1-weighted scan was acquired for all subjects. The cortical surface of each hemisphere was algorithmically reconstructed from this anatomical volume using FreeSurfer software (http://surfer.nmr.mgh. harvard.edu/, Version 5.3.0) (Dale et al., 1999). All T2*-weighted EPI (BOLD) images were acquired using a slice-accelerated EPI sequence that permits simultaneous multislice acquisitions using the blipped-CAIPI technique (Setsompop et al., 2012). A total of 69 2 mm slices were collected (0% skip) with a slice acceleration factor of 3 (TE 30 ms; TR 2 s; flip angle = 80°; 6/8 partial-fourier acquisition), covering the whole brain. Images were acquired at a nominal 2 mm isotropic spatial resolution (matrix size = 108 × 108 × 69).

2.2.1. Visual vs. auditory working memory 2-back & resting-state

14 subjects participated in two sets of MRI scans collected in two separate sessions. In the first session, structural MRI scans were collected to support anatomical reconstruction of the cortical surfaces. In the second session, we acquired eight runs of functional data, with each run comprising two blocks of a visual 2-back working memory task, two blocks of an auditory 2-back working memory task, and two blocks each of visual and auditory sensorimotor control. Each block lasted 40 s and comprised 32 stimulus presentations. In addition, 8 s of fixation was collected at the beginning, midpoint, and end of each run. Subjects also underwent two or three runs of resting-state fMRI (180 TRs, 6 min duration) with identical scan parameters.

2.2.2. Visual working memory change-detection (VWM-cd) & multiple object tracking (MOT)

For VWM-cd, each subject completed eight runs (total time per run = 6 min 16 s). Each run comprised ten 34 s task blocks and 16 s of blank fixation before the first block and after the last block. Each block consisted of a 2 s cue, which indicated the location of the target stimuli (left or right hemifield), followed by eight 4 s trials. For MOT, subjects completed four runs (total time per run = 4 min 56 s), comprising 16 alternating active and sensorimotor control blocks, each lasting 18 s. The 4 s of blank fixation was presented before and after the task blocks.

2.3. Stimuli and experimental paradigms

2.3.1. Visual vs. auditory working memory 2-back & resting-state

All stimuli were created in MATLAB (The MathWorks) using the Psychophysics Toolbox extension (Brainard, 1997; Pelli, 1997) and were presented using a liquid crystal display projector illuminating a rear-projection screen within the scanner bore. Subjects performed a 2-back working memory task on visual and auditory stimuli, in separate blocks. Visual stimuli were black-and-white photographs of young adult faces, each presented for 1 s with a 0.25 s inter-stimulus interval. To make the 2-back task more challenging and less amenable to a verbal labeling strategy, photographs of men and women were presented during separate blocks. Images were presented at 300 × 300 pixels, spanning ~6.4° visual angle. Auditory stimuli were natural recordings of cat and dog vocalizations, collected from sound effects files freely available on the web. Recordings of cats and dogs were included in separate blocks, again to increase task difficulty and discourage verbal labeling strategies. Auditory stimuli lasted 300–600 ms, and the onsets of successive stimuli were separated by 1.25 s (matching the timing of the visual stimuli). Stimuli were presented diotically. The audio presentation system (Sensimetrics, http://www.sens.com) included an audio amplifier, S14 transformer, and MR-compatible in-ear earphones.

At the beginning of each block, a visual cue indicated whether the block would entail a 2-back WM task (“auditory 2-back,” “visual 2-back”) or a sensorimotor control (“auditory passive,” “visual passive”). Block order was counterbalanced across runs; run order was counterbalanced across subjects. During 2-back blocks, participants were instructed to decide whether each stimulus was an exact repeat of the stimulus two prior, and to indicate either a “2-back repeat” or “new” stimulus via button press. Sensorimotor control blocks consisted of the same stimuli and timing, but lacked 2-back repeats, and participants were instructed to

make a random button press to each stimulus. The contrast of visual working memory > auditory working memory (blocks of each 2-back condition) was used to define frontal ROIs in each individual subject. Subjects also participated in resting-state scans, in which they were instructed to keep their eyes open, maintain fixation on a centrally located crosshair, and allow their minds to wander. The task-defined ROIs were employed in resting-state analysis (see section 2.5 below).

2.3.2. Visual working memory change-detection (VWM-cd)

Stimuli were generated and presented using MATLAB (The MathWorks) using the Psychophysics Toolbox extension (Brainard, 1997; Pelli, 1997). Subjects fixated on a centrally located cross while 12 oriented colored bars were presented (6 in each hemifield). The number of bars presented in each hemifield remained constant across trials, but the number of memory targets presented on a given trial was either 1 or 4. The remaining bars in the display served as distractors. Targets and distractors were distinguished by color, with targets denoted by red and distractors denoted by blue. Each bar subtended 0.25° × 2.5° of visual angle. Targets were limited to either the right or left hemifield (counterbalanced across blocks). Subjects were instructed to remember the orientation (0°, 45°, 90°, 135°) of the target items in the display. The memory sample display was presented for 200 ms followed by a 1000 ms delay period. After the sample and delay period, a memory probe was presented for 1800 ms. A 1000 ms fixation period separated each trial. On half of the trials, one of the target bars changed its orientation from the sample period to probe period. On the other half of the trials, the memory probe array was identical to the sample array (distractors never changed). Subjects could respond during either the memory probe or the inter-trial fixation period by pressing a key to indicate that the orientation of a target had changed, or a separate key if it had not changed. The magnitude of the change was always 90° (e.g., 0°–90° or 45°–135°). During sensorimotor control trials, subjects were presented a display consisting entirely of distractors and were instructed to press either key during the probe or inter-trial fixation period. All subjects possessed extensive experience at performing psychophysical tasks while maintaining fixation on a central crosshair. In-scanner eye tracking confirmed that subjects tightly held central fixation through all conditions; there was no significant difference between attend-left and attend-right trials in root-mean-square (RMS) deviation from fixation ($t(7) = 0.84$; $p = 0.43$) or horizontal eye position ($t(7) = 1.54$; $p = 0.17$).

2.3.3. Multiple object tracking (MOT)

Stimuli were generated and presented using Python with the VisionEgg software package (Straw, 2008; Bettencourt et al., 2011). The display consisted of two spatially offset rectangular regions, one per hemifield, each containing six white disks and a centrally located crosshair. At the onset of each trial, four target disks were highlighted in red for 1500 ms before changing back to white for 500 ms. Following the cue period, all disks in the display moved in random directions at a constant speed of 4.8°/s for 12 s. Disks repulsed off other disks and the hemifield display edges, preventing any overlap. Subjects were instructed to maintain fixation on the central crosshair and to covertly attend to the cued target disks as they moved around the display. All subjects possessed extensive experience in performing psychophysical tasks while maintaining fixation on a central crosshair. To further encourage subjects to maintain central fixation, two targets were restricted to the left visual hemifield and two were restricted to the right visual hemifield. Once the disks stopped moving, a single disk was highlighted in blue for 3000 ms. Subjects were asked to respond by pressing a key if the probed disk was one of the original targets, or to press a separate key if it was not a target. A 1000 ms blank fixation interval separated each trial. At the onset of sensorimotor control trials, every disk in the display was highlighted in red during the cue period. In this condition, subjects were instructed to refrain from tracking the disks and to press either key during the probe period. Subjects practiced the task before scanning.

2.4. MRI data analysis & preprocessing

Functional data were analyzed using the FreeSurfer/FS-FAST pipeline (Charlestown; http://surfer.nmr.mgh.harvard.edu/) (Fischl, 2012). All data and code used for data analysis are available upon request. Further information and requests for resources should be directed to and will be fulfilled by the Lead Contact, David C. Somers (somers@bu.edu).

2.4.1. Visual vs. auditory working memory

Subject data were registered to the individual's anatomical data using the middle time point of the functional data, motion corrected by run, slice-time corrected, intensity normalized, re-sampled onto the individual's cortical surface (voxels to vertices), and spatially smoothed (3 mm FWHM). The GLM analysis used standard procedures within FreeSurfer/FS-FAST (version 5.3.0). Scan time series were analyzed vertex by vertex on the surface using a GLM with regressors matching the time course of the experimental conditions. The time points of the cue period were excluded by assigning them to a regressor of no interest. A canonical hemodynamic response function was convolved with the regressors before fitting; this canonical response was modeled by a gamma function ($\delta = 2.25$ s, $\tau = 1.25$) (Boynton et al., 1996). Contrasts between conditions produced t-statistics for each vertex for each subject.

2.4.2. Resting-state

Resting-state data were preprocessed in a manner similar to that of the visual vs. auditory WM task data. Multiple resting-state acquisitions for each subject were temporally demeaned and concatenated to create a single timeseries. In order to attenuate artifacts that could induce spurious correlations, resting-state data were further preprocessed using custom scripts in MATLAB. The following preprocessing steps were performed: linear interpolation across high-motion time-points (>0.5 mm FD; Power et al., 2012; Carp, 2013), application of a fourth-order Butterworth temporal bandpass filter to extract frequencies between 0.009 and 0.08 Hz, mean 'grayordinate' signal regression (MGSR; Burgess et al., 2016), and censoring of high-motion time-points (Power et al., 2012).

2.4.3. Visual working memory change-detection (VWM-cd) & multiple object tracking (MOT)

The preprocessing procedure implemented here was identical to that used for the visual vs. auditory working memory task. Additionally, data were spatially co-registered to the FreeSurfer "fsaverage" brain to enable aggregation over subjects. Single-subject data were then analyzed voxelwise using a general linear model that included a predictor for each task condition (VWM-cd: set size 1, set size 4, sensorimotor control; MOT: active tracking and sensorimotor control). To control for activation due to cue reorientation, cue time points were included as nuisance regressors in the model. To compare differences in activation between conditions, group statistical maps were generated using voxel-wise t-tests with variance smoothing ($\sigma = 4$ mm). For VWM-cd, the set size 4 condition was contrasted against the sensorimotor control condition; for MOT, the active tracking condition (set size 4) was contrasted against the sensorimotor control condition.

To correct for multiple comparisons, we employed nonparametric randomization tests (Nichols and Holmes, 2002) and threshold-free cluster enhancement (TFCE) transformation (Smith and Nichols, 2009). For each group statistical map, the image-wise maximum TFCE statistic was recorded for all possible permutations or sign-flips ($n = 2^{\wedge}9$ or 512), and used to generate a null distribution. Using this null distribution, original group maps were thresholded at $p < 0.05$, one-sided.

2.5. LFC seed differential functional connectivity analysis

2.5.1. Visual-biased LFC ROI definition

Using data obtained from the visual vs. auditory working memory task (Noyce et al., 2017), visual-biased frontal cortical ROIs were defined

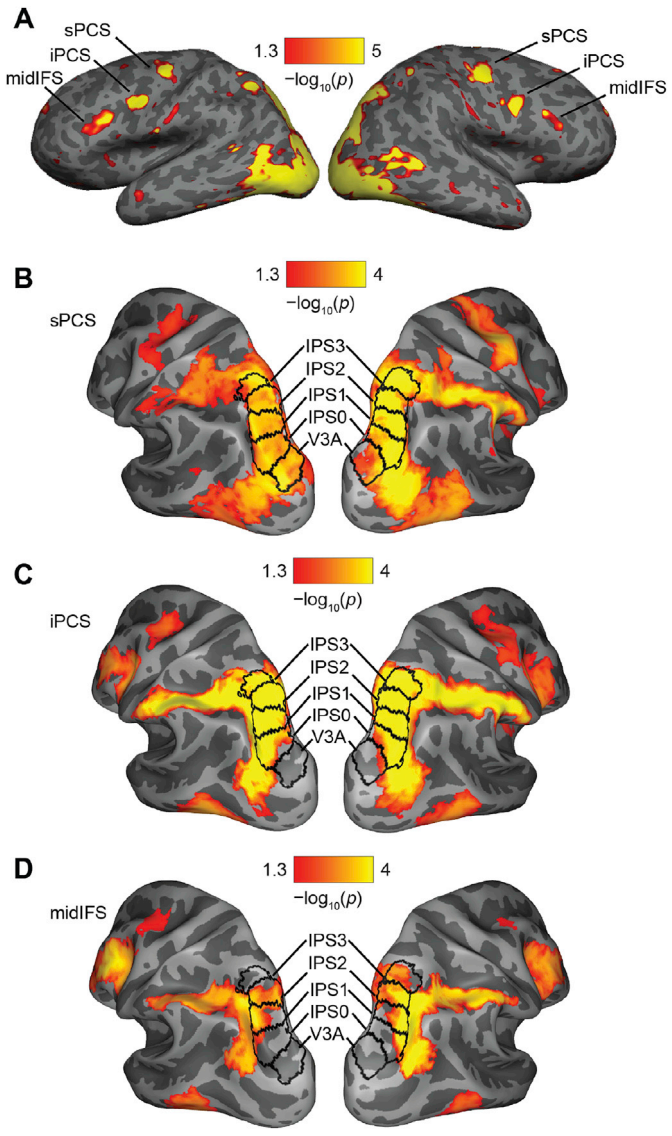

Fig. 1. Seed-based rsFC for visual-biased LFC regions.
(A) LFC visual cognition structures sPCS, iPCS, and midIFS were identified from a contrast of 2-back visual WM with 2-back auditory WM task activation (Noyce et al., 2017, 2018). Individual subject ROIs were used as seed regions in rsFC analysis. Representative data from one individual subject. (B–D) Group-average seed-to-vertex rsFC results (n = 14) for each of the three LFC ROIs. Family-wise error rate was controlled at 0.05 using permutation tests with threshold-free cluster enhancement. Probabilistic areal boundaries for retinotopic areas V3A and IPS0-3 (Wang et al., 2015) are overlaid.

for each individual subject based on the direct contrast of blocks in which the subject performed visual WM against blocks in which the subject performed auditory WM. Prior to ROI definition, this contrast (visual WM > auditory WM) was liberally thresholded at p = 0.05, uncorrected, and cortical significance maps underwent additional smoothing using the FreeSurfer visualization toolkit (five iterations of a box kernel). As described in Noyce et al. (2017, 2018), these data were used in combination with anatomical constraints to define three bilateral LFC ROIs (sPCS, iPCS, midIFS; see Fig. 1A). Each ROI was required to lie in the expected anatomical region (e.g., on the superior precentral sulcus), exhibit a visual > auditory task contrast, and interleave with auditory-biased regions. To generate probabilistic ROIs, visual-biased labels for each subject were projected to "fsaverage" space. For each LFC ROI, vertices that appeared in the label of 3 or more subjects (20% of the participants) were incorporated into a probabilistic region of interest.

2.5.2. Seed-based resting state functional connectivity

For each seed ROI in each individual subject hemisphere, we calculated a mean time course for all vertices within the ROI. Each LFC ROI time course was then correlated with that of every vertex in the cerebral cortex ipsilateral to the ROI. Resulting correlation maps for each subject were registered to the FreeSurfer "fsaverage" template surface space, subjected to Fisher's *r*-to-*z* transformation, and then submitted to a 2nd-level group analysis. To correct for multiple comparisons, we employed threshold free cluster enhancement (TFCE) and non-parametric randomization tests in a manner similar to that employed for the task analysis (see section 2.4.3) and used these results to create significance masks for each analysis. That is, masks came from task activation that survived correction. Identical functional connectivity analyses were conducted using composite seeds that comprised all pairwise combinations of the three seeds (sPCS + iPCS, sPCS + midIFS, iPCS + midIFS). These were used to generate the three-way functional connectivity comparison map, described below.

2.5.3. Differential resting state functional connectivity

Before undergoing a difference analysis, all uncorrected vertex-wise group *z*-statistic maps were standardized across each cortical hemisphere; this allowed for the direct comparison of effect size between any two maps. Standardization was accomplished by subtracting from each vertex in the map the mean *z*-statistic of all vertices across the hemisphere, and then dividing by the standard deviation.

Two-way difference maps (sPCS – iPCS, sPCS – midIFS, iPCS – midIFS) were created via subtraction, and each resulting difference map was FWE-corrected via the exclusion of all vertices that did not survive multiple comparisons in both single-seed functional connectivity analyses (Brissenden et al., 2018); that is, only vertices present in at least one significance mask were included. To compare the functional connectivity of all three LFC ROIs (sPCS, iPCS, midIFS), we subtracted from each ROI's functional connectivity map that of the composite seed comprising the other two ROIs. Each resulting difference map included only the vertices that survived multiple comparison correction, with positive correlation in at least one of the three single-seed functional connectivity analyses. In each hemisphere, the three resulting Z-score difference maps (sPCS – (iPCS + midIFS), iPCS – (sPCS + midIFS), midIFS – (sPCS + iPCS)) were subjected to min-max scaling; this allowed us to use each vertex's three contrast values, ranging from 0 to 1, as an RGB triplet (Red, sPCS; Green, iPCS; Blue, midIFS) for simultaneous visualization in MATLAB. "Winner-take-all" maps were constructed by converting each vertex to pure hue red, green, or blue, depending on the LFC ROI to which it exhibited the strongest relative connectivity. Parietal ROIs used for the probability density analysis and VWM-cd vs. MOT task analyses (described below) were created by excluding from each of the "winner-take-all" maps (red, green, and blue) all vertices outside of superior and inferior parietal cortex as defined by the Desikan-Killiany brain atlas (Desikan et al., 2006). These parietal ROIs defined by the 'winner-take-all' analysis of functional connectivity with LFC regions were defined as p-sPCS, p-iPCS, p-midIFS, respectively.

In order to quantify the spatial organization of selective parietal connectivity with our LFC ROIs, we examined the distribution across space of the vertices connected most strongly with each LFC ROI, as defined by the "winner-take-all" parietal ROIs described above. We extracted the anatomical right/left, anterior/posterior, and superior/inferior coordinates (as FreeSurfer "RAS" coordinates) for each vertex and computed the probability density function across space for vertices classified as sPCS-, iPCS-, or midIFS-selective. To examine the organization of sPCS vs. iPCS resting state functional connectivity along retinotopic IPS, we examined the V3A and IPS0-4 regions as defined by the Wang et al. (2015) probabilistic retinotopy atlas.

2.6. Differential task recruitment analysis

To contrast VWM-cd and MOT task activation, we conducted a

difference analysis similar to that used to compare seed-based functional connectivity maps. In order to directly compare cortical activation evoked by two different tasks, uncorrected group *t*-statistic maps for MOT (active tracking > sensorimotor control contrast) and VWM-cd (set size 4 > sensorimotor control contrast) were standardized across ipsilateral cortex by subtracting the mean *t*-statistic and dividing by the standard deviation. Task activation maps were then contrasted against each other by subtraction. To correct for multiple comparisons, the resulting difference map included only vertices that survived multiple comparison correction (see section 2.4) in at least one task analysis. Individual-subject (n = 3) task difference analyses used a similar process, and the same vertices (those that did not survive multiple comparison correction in the group analyses) were excluded.

As specified earlier, parietal ROIs (p-sPCS, p-iPCS, p-midIFS) used for the VWM-cd vs. MOT task analyses were created by excluding from each of the "winner-take-all" maps (see section 2.5) all vertices outside of superior and inferior parietal cortex as defined by the Desikan-Killiany brain atlas (Desikan et al., 2006). To analyze VWM-cd and MOT task data in LFC, probabilistic visual-biased frontal ROIs (sPCS, iPCS, midIFS) were defined, as described above. To compare differential task activation between ROIs, we extracted from each ROI the mean effect size from each standardized task activation map (VWM-cd and MOT). Differences in task-specificity between ROIs were examined using a linear mixed effects model. The model was fitted using the lme4 package (version 1.1–10; Bates et al., 2015). To account for within-subject error covariance, the model included a random effect associated with the intercept for each subject. Denominator degrees of freedom and p-values were computed using the Satterthwaite approximation as implemented by the lmerTest package (version 2.0–32; Kuznetsova et al., 2017). Within an ROI, pairwise comparisons between tasks were performed using the lsmeans package (version 2.25; Lenth, 2016).

3. Results

3.1. Differential functional connectivity gradients within frontoparietal visual attention network

We examined the intrinsic resting-state functional connectivity of three lateral frontal visual attention regions, superior precentral sulcus (sPCS), inferior precentral sulcus (iPCS), and the middle portion of inferior frontal sulcus (midIFS), with parieto-occipital cortex. Seed ROIs (sPCS, iPCS, and midIFS) in each hemisphere were drawn in 14 individual subjects based on the contrast of visual vs. auditory working memory task recruitment (visual > auditory; Fig. 1A; Noyce et al., 2017). For each ROI in each subject, we extracted the average resting-state time course and then computed its correlation with the resting-state time course of every vertex in the ipsilateral hemisphere. Individual subject correlation maps were then Fisher's z-transformed and submitted to a 2nd-level group analysis. Family-wise error rate was controlled at 0.05 using permutation tests with threshold-free cluster enhancement (TFCE) (see 2.4.3, 2.5.2; Nichols and Holmes, 2002; Smith and Nichols, 2009; Eklund et al., 2016).

Each of the frontal cortical ROIs demonstrated strong intrinsic functional connectivity with posterior parietal cortex, including regions along intraparietal sulcus (IPS) and superior parietal lobule (SPL) (Fig. 1B-D). Despite the similarities in parietal connectivity for each frontal ROI, differences were evident upon closer inspection both in the group and individual subject patterns (see Supplemental Figure 1). Prior fMRI studies have demonstrated the existence of multiple parieto-occipital regions which each contain topographically organized representations of the contralateral visual field (Sereno, 2001; Silver et al., 2005; Swisher et al., 2007; Konen and Kastner, 2008). We examined LFC connectivity to probabilistic ROIs (Wang et al., 2015) for retinotopically defined parieto-occipital regions V3A, IPS0, IPS1, IPS2, and IPS3 (Table 1). This revealed a significant main effect of ROI ($F(2,401.25) = 38.09$, $p < 0.0001$) and of hemisphere (RH > LH: $F(1,401.25) = 3.92$, $p = 0.048$), but no interaction between hemisphere and ROI ($F(2,401.25) = 0.016$, $p = 0.98$). *Post hoc* comparisons revealed that connectivity from midIFS to the retinotopic ROIs was weaker than that of sPCS and iPCS (sPCS: $t(401.7) = 7.95$, iPCS: $t(401.7) = 7.15$; both $p < 0.0001$, corrected). We found that sPCS and iPCS connectivity were roughly uniform across IPS regions ($t(400.9) = 0.80$; $p = 0.4226$), with the exception of V3A, where sPCS connectivity was robust, but iPCS connectivity was weak in both hemispheres (main effect of ROI $F(1,42) = 8.12$, $p = 0.0067$).

Table 1
Average correlation of LFC ROIs with retinotopic IPS ROIs. From each retinotopic IPS ROI as defined by Wang et al. (2015), average correlation values (r) and s.e.m. were extracted from the uncorrected group-average seed-to-vertex rsFC map of each LFC ROI.

LFC ROI	Hemi	V3A	IPS0	IPS1	IPS2	IPS3
sPCS	L	0.22 ± 0.05	0.23 ± 0.05	0.26 ± 0.06	0.24 ± 0.05	0.28 ± 0.06
	R	0.17 ± 0.06	0.31 ± 0.05	0.29 ± 0.05	0.30 ± 0.05	0.30 ± 0.05
iPCS	L	0.05 ± 0.05	0.25 ± 0.05	0.30 ± 0.04	0.27 ± 0.03	0.26 ± 0.05
	R	0.09 ± 0.05	0.30 ± 0.05	0.32 ± 0.04	0.30 ± 0.04	0.29 ± 0.04
midIFS	L	−0.08 ± 0.04	0.06 ± 0.05	0.19 ± 0.04	0.16 ± 0.04	0.05 ± 0.03
	R	−0.08 ± 0.03	0.09 ± 0.04	0.19 ± 0.04	0.21 ± 0.04	0.13 ± 0.04

From each retinotopic IPS ROI as defined by Wang et al. (2015)., average correlation values (r) and s.e.m. were extracted from the uncorrected group-average seed-to-vertex rsFC map of each LFC ROI.

To further assess the functional connectivity differences across frontal seeds, we standardized the uncorrected group statistic map of each frontal seed across cortex to create an effect size map. In order to combine all three into a single map (Fig. 2A), we then contrasted (within hemisphere, via subtraction) each seed's connectivity effect size map against that of a composite seed comprising the other two ROIs. Each resulting difference map included only the vertices that survived multiple comparison correction in at least one of the three single-seed functional connectivity analyses. The differences in vertex Z-scores were then arranged into a 3-element vector and scaled to create an RGB code in which red signified greater connectivity with sPCS than with the combined iPCS and midIFS seed; in the same manner, green and blue represented greater connectivity with iPCS and midIFS, respectively.

The three-way contrast of sPCS, iPCS, and midIFS functional connectivity revealed a dorsomedial to ventrolateral connectivity gradient in parieto-occipital cortex: relative to the other two seeds, sPCS connectivity was dominant in dorsal SPL, anterior SPL, and extrastriate cortex; iPCS connectivity was dominant near the fundus of IPS; midIFS connectivity was dominant in the lateral bank of IPS. Note that this gradient runs approximately orthogonal to the organization of the swath of visuotopic parietal ROIs examined in Table 1. This shift was especially apparent after a "winner-take-all" analysis, in which each vertex was converted to pure hue red (sPCS), green (iPCS), or blue (midIFS) depending on the ROI to which it exhibited the strongest standardized connectivity (Fig. 2B; see also Supplemental Fig. 2). Three, nested, crescent-shaped regions that run parallel to the intraparietal sulcus clearly stand out on the inflated cortical hemispheres. The region of sPCS-dominant connectivity extended rostrally from IPS3 along the anterior branch of IPS and also ventrolaterally from area V3A. Additionally, midIFS dominated in a small dorsomedial region medial to the probabilistic definition of IPS2. Although outside the primary focus of this investigation, lateral occipitotemporal cortex also exhibits an sPCS-to-iPCS-to-midIFS functional connectivity gradient running anteroventrally.

Closer examination of the differential patterns of frontal lobe connectivity to parietal cortex reveals finer structure within the parietal regions that exhibit retinotopic maps (Fig. 2A and B). This is most evident

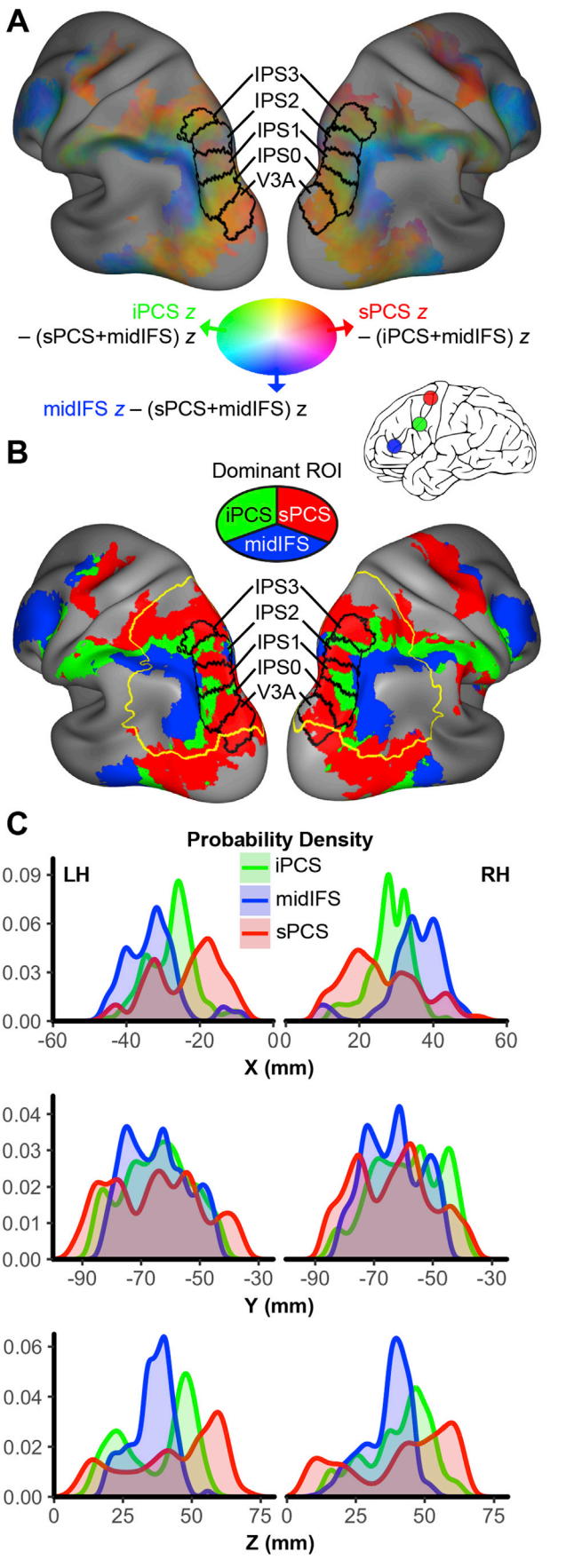

(caption on next column)

Fig. 2. Differential rsFC in visual fronto-parietal cortex. (A) Group-level (n = 14) standardized three-way comparison of seed-to-vertex rsFC from each LFC ROI (sPCS, iPCS, and midIFS) reveals a dorsomedial to ventrolateral gradient in parieto-occipital cortex. R (sPCS), G (iPCS), or B (midIFS) values generated by subtracting from each ROI's rsFC map that of a composite seed comprising the other two ROIs. (B) "Winner-take-all" map in which vertices were assigned pure hue R, G, or B depending on the ROI to which they were most strongly connected. Yellow areal boundaries illustrate a lateral parietal ROI defined by combining superior and inferior parietal cortex parcels from an anatomical atlas (Desikan et al., 2006). (C) Probability density curves for rsFC with each parietal ROI demonstrate a shift (sPCS to iPCS to midIFS) along the X and Z dimensions.

in the differential patterns of connectivity from sPCS and iPCS frontal seeds to parietal cortex (also see Fig. 4B). iPCS connectivity is relatively stronger at the IPS0/IPS1 boundary and near the IPS2/IPS3 boundary (as defined by the Wang atlas), especially in the more lateral portions of these boundaries, whereas sPCS connectivity appears relatively stronger elsewhere within IPS0-3. This pattern is strongly symmetric between the hemispheres and corresponds to the known retinotopic organization of parietal cortex (Swisher et al., 2007; Mackey et al., 2017) which exhibits two foveal representations in IPS, one at the lateral side of the IPS0/1 border and another at the lateral side of side of the IPS2/3 border. Foveal representations are confluent between neighboring cortical areas and have been suggested to form the center of visual map field clusters composed of multiple regions (Wandell et al., 2007; Mackey et al., 2017). These observations suggest that iPCS connectivity to retinotopic parietal regions is biased toward foveal representations of the visual field, while sPCS connectivity is biased toward peripheral visual field representations in parietal cortex. Additionally, the IPS0/1 border and IPS2/3 border represent the lower visual field meridian, while the neighboring borders between IPS regions represent the upper visual field meridian. This suggests a possible lower visual field bias for iPCS connectivity relative to an upper visual field bias for sPCS connectivity.

To quantify the anatomical differences of each seed's parietal functional connectivity, we masked the winner-take-all map to exclude vertices outside of parietal cortex (using anatomical definitions of superior parietal and inferior parietal cortex from Desikan et al., 2006; mask indicated by yellow border in Fig. 2B), then used it to create probability density functions for sPCS-, iPCS-, and midIFS-dominant vertices for each of the right/left, anterior/posterior, and superior/-inferior anatomical axes ("RAS" coordinates in FreeSurfer surface files) (Fig. 2C). These analyses revealed clear gradients of connectivity (sPCS to iPCS to midIFS) along both mediolateral (medial to lateral) and dorsoventral (dorsal to ventral) axes. The global peaks (modes) in the density function, along with the mean coordinates for each ROI, follow a systematic medial to lateral shift (right/left axis mode and mean for right hemisphere [RH]: sPCS = 19.7, 26.2; iPCS = 27.8, 28.3; midIFS = 34.2, 34.9; left hemisphere [LH:] sPCS = −17.9, −23.6; iPCS = −25.9, −27.6; midIFS = −31.8, −32.9). A shift is also observed in the superior/inferior axis ([RH:] sPCS = 59.5, 40.8; iPCS = 46.7, 40.5; midIFS = 39.7, 36.5; [LH:] sPCS = 59.3, 42.4; iPCS = 47.8, 37.3; midIFS = 39.9, 36.5). The anteroposterior axis exhibited multiple peaks and troughs with iPCS peaks corresponding to sPCS troughs, and vice versa (reflecting the boundaries between IPS regions, as noted above), but the mean locations did not show obvious distinctions between populations ([RH:] sPCS = −57.7, −63.7; iPCS = −54.3, −59.0; midIFS = −61.4, −63.4; [LH:] sPCS = −63.9, −65.3; iPCS = −62.3, −64.7; midIFS = −74.9, −64.7).

3.2. *Differential parietal connectivity of LFC ROIs mirrors differential spatial attention and visual WM task recruitment*

In order to examine the functional significance of these network differences, we assessed recruitment of these LFC-connected parietal structures during two different visual cognitive processing paradigms: a visual spatial attention multiple object tracking (MOT) task and a visual working memory change-detection (VWM-cd) task (note that frontal ROI

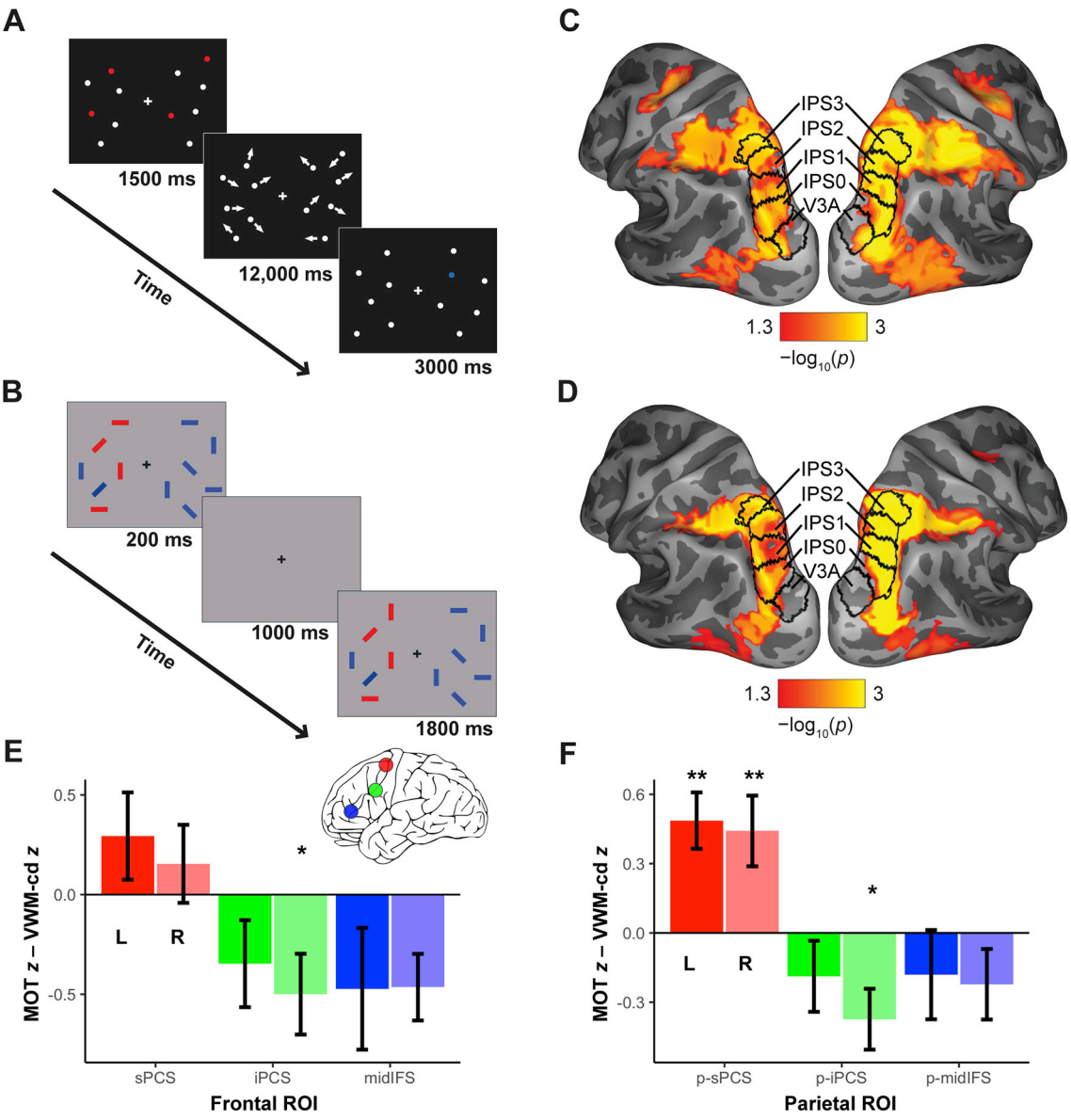

Fig. 3. Significant interaction of task and ROI. (A) Multiple object tracking (MOT) paradigm and (B) Visual working memory change detection (VWM-cd) paradigm (see Methods 2.3.2, 2.3.3). (C) Group-level MOT task activation (n = 9; TFCE permutation tests, $p < 0.05$), contrasting the active tracking condition against the sensorimotor control condition. (D) Group-level VWM-cd task activation (n = 9; TFCE permutation tests, $p < 0.05$), contrasting the set size 4 condition against the sensorimotor control condition. (E–F) Bars represent the difference in mean effect size between MOT and VWM-cd activation in (E) probabilistic LFC ROIs and (F) parietal regions most strongly connected to each ROI (R, G, and B ROIs within the parietal mask in Fig. 2B). Error bars indicate a bootstrapped estimate of SEM (100 bootstraps). In sPCS and p-sPCS, mean MOT effect size exceeds mean VWM-cd effect size; the opposite is true for all other ROIs.

definitions do not derive from either task). These specific tasks were selected for analysis because prior work from our laboratory observed differences in lateral frontal cortical activity between these tasks, with more robust activity in the vicinity of sPCS for the MOT task and more robust activity in the vicinity of iPCS and midIFS for the VWM-cd task (Brissenden et al., 2016). Given this observation, we hypothesized that these tasks would exhibit parallel differences in posterior parietal activation, in line with the differential functional connectivity patterns.

In the MOT task, participants (n = 9) maintained central fixation while tracking the trajectory of four targets (white disks), which moved randomly around a display along with four identical distractor disks (see Methods 2.3.3 and Fig. 3A). In the VWM-cd task, participants (n = 9, with n = 4 participant-overlap with MOT task) maintained central fixation and were required to maintain in working memory the orientation of four briefly-presented target items (red bars) (see Methods 2.3.2 & Fig. 3B). To assess regions recruited during visual working memory and multiple object tracking, each of these task conditions were contrasted against sensorimotor control conditions in which the stimuli were equivalent to their respective 4-item load conditions, but no items were stored in working memory or attentively tracked. To correct for multiple comparisons, we employed permutation-based nonparametric randomization tests (Nichols and Holmes, 2002) and threshold free cluster enhancement (TFCE) transformation (Smith and Nichols, 2009), thresholded at $p < 0.05$, one-sided. Both MOT and VWM-cd tasks broadly and bilaterally recruited regions in parieto-occipital cortex, including extrastriate cortex, medial IPS, lateral IPS, and dorsal SPL. Parietal activation looks broadly similar across both visual cognition contrasts, but closer inspection reveals fine-scale differences (Fig. 3C and D), with MOT activity shifted dorsomedially relative to VWM-cd activity.

In order to analytically confirm our prior observation of differential lateral frontal activity for these two tasks, we extracted mean effect size in each subject from each of the frontal ROIs (midIFS, iPCS, and sPCS),

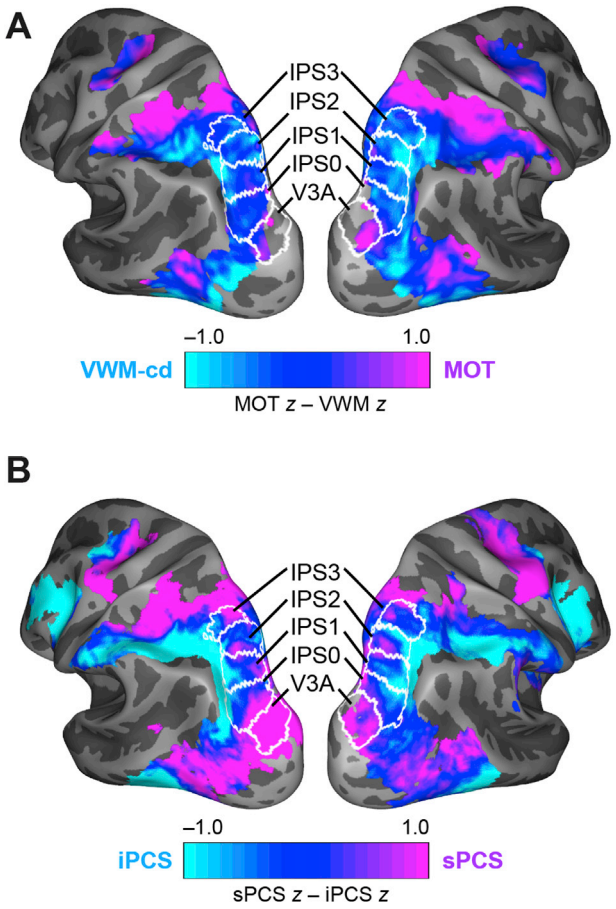

Fig. 4. Task differences mirror rsFC gradient in parieto-occipital cortex. (A) Standardized comparison of MOT (n = 9) with VWM-cd (n = 9) task activation reveals a dorsomedial to ventrolateral gradient in parieto-occipital cortex. (B) Standardized comparison of sPCS seed-to-vertex rsFC with iPCS seed-to-vertex rsFC (n = 14) reveals a similar gradient.

defined probabilistically across subjects from Noyce et al. (2017 ,2018), (3 subjects shared with the MOT and VWM-cd tasks). These data were entered into a linear mixed effects model, with fixed effects of hemisphere, ROI, task, plus their interactions, and a random effect of subject ID. This revealed a significant interaction between task and ROI ($F(2, 108) = 5.92$, $p = 0.0362$), suggesting task selectivity in the LFC ROIs. *Post hoc* comparisons revealed that VWM-cd elicited greater percent signal change (vs. MOT) in right iPCS ($t(25.6) = -2.34$, $p = 0.0276$ corrected); this comparison approaches significance in left and right midIFS (Left: $t(29.9) = -1.98$, $p = 0.0568$ corrected; Right: $t(29.9) = -1.95$, $p = 0.0608$ corrected). Mean percent signal change was numerically greater for MOT in sPCS bilaterally, and VWM-cd for left iPCS, but these differences did not achieve statistical significance (Fig. 3E. Other significant effects include an interaction between hemisphere and ROI ($F(2,108) = 3.36$, $p = 0.0385$), and main effects of task ($F(1,108) = 5.86$, $p = 0.0172$) and ROI ($F(2,108) = 64.81$, $p < 0.0001$) (Table 2).

The same analysis was performed for each "winner-take-all" parietal ROI defined by functional connectivity to each frontal seed (see Fig. 2C), here referred to as p-sPCS, p-iPCS, and p-midIFS. The mixed effects model revealed a significant interaction between task and ROI ($F(2,90) = 18.25$, $p < 0.0001$, revealing robust differences in visual task selectivity between p-sPCS, p-iPCS, and p-midIFS. *Post hoc* comparisons revealed that MOT elicited a greater effect than VWM-cd in p-sPCS right ($t(21.4) = 3.22$, $p = 0.004$, Holm-Bonferroni corrected) and p-sPCS left ($t(21.4) = 3.55$, $p = 0.0019$ corrected), whereas VWM-cd exhibited greater activation than MOT in p-iPCS right ($t(25.9) = -2.67$, $p = 0.0130$ corrected). Mean effect size was numerically greater for VWM-cd (vs. MOT) in left p-iPCS and left and right p-midIFS, but did not achieve statistical significance (Fig. 3F). Other significant effects include an interaction between hemisphere and ROI ($F(2,90) = 5.49$, $p = 0.0056$), and main effects of hemisphere ($F(1,90) = 8.92$, $p = 0.0036$) and ROI ($F(1,90) = 8.92$, $p = 0.0036$) (Table 2). The broad pattern in both lateral frontal cortex and posterior parietal cortex exhibits relatively greater MOT activation in more dorsal regions and relatively greater VWM-cd activation in more ventral regions.

Table 2
Regions of interest, percent signal change (PSC) by task, and statistics for task comparison.

Frontal	Hemi	MOT (PSC)	VWM-cd (PSC)	t	p
sPCS	LH	1.63 ± 0.14	1.34 ± 0.21	1.32	0.1957
	RH	1.43 ± 0.06	1.27 ± 0.21	0.69	0.4931
iPCS	LH	0.70 ± 0.15	1.04 ± 0.18	−1.62	0.1171
	RH	0.77 ± 0.14	1.27 ± 0.16	−2.34	0.0276 *
midIFS	LH	−0.31 ± 0.18	0.16 ± 0.25	−1.98	0.0568 .
	RH	0.14 ± 0.13	0.61 ± 0.13	−1.95	0.0608 .
Parietal					
p-sPCS	LH	1.62 ± 0.08	1.13 ± 0.10	3.55	0.0019 **
	RH	1.56 ± 0.09	1.12 ± 0.13	3.22	0.0040 **
p-iPCS	LH	1.80 ± 0.11	1.98 ± 0.12	−1.34	0.1920
	RH	1.82 ± 0.11	2.20 ± 0.07	−2.67	0.0130 *
p-midIFS	LH	0.27 ± 0.11	0.45 ± 0.16	−1.064	0.2960
	RH	0.66 ± 0.09	0.88 ± 0.14	−1.31	0.2003

In order to more finely reveal the relative task recruitment differences in posterior parietal cortex, we standardized the uncorrected group statistic map of each analysis (Fig. 3C and D), contrasted each standardized task recruitment map via subtraction (VWM-cd – MOT), and excluded vertices that did not survive multiple comparison correction in at least one task (Fig. 4A). VWM-cd activation was relatively stronger in ventrolateral portions in posterior parietal cortex, especially along the lateral bank of the intraparietal sulcus. MOT was relatively stronger in area V3A and in the regions anterior to IPS3. Within IPS0 to IPS3, small domains of VWM-cd preference and MOT preference were interleaved. The pattern of contrasted task results closely mirrors the contrasted functional connectivity results. To examine this relationship from a continuous rather than discrete perspective, we computed the spatial correlation within parietal cortex between the MOT vs. VWM-cd difference map and each of the possible two-way difference analyses of the standardized and FWE-corrected group-level connectivity maps for each frontal seed (i.e., sPCS – iPCS, sPCS – midIFS, iPCS – midIFS). The sPCS vs. iPCS comparison (Fig. 4B) yielded the strongest correlations for each hemisphere ([RH]: $r = 0.61$, $p < 0.0001$; [LH]: $r = 0.65$, $p < 0.0001$), however positive correlations were also observed for sPCS vs. midIFS ([RH]: $r = 0.48$, $p < 0.0001$; [LH]: $r = 0.52$, $p < 0.0001$) and iPCS vs. midIFS ([RH]: $r = 0.28$, $p < 0.0001$; [LH]: $r = 0.38$, $p < 0.0001$).

Given that the MOT and VWM-cd datasets contain two distinct subject pools, we sought to confirm that the parietal gradient revealed in the group contrast replicates in each of the three subjects for whom we collected resting-state, MOT, and VWM-cd data. This was indeed the case, as each individual subject exhibited a similar pattern: stronger MOT recruitment in dorsomedial IPS and dorsal SPL, and stronger VWM-cd recruitment in ventrolateral IPS (Fig. 5).

These results demonstrate that the differential patterns of frontoparietal functional connectivity effectively capture the differences in parietal lobe recruitment between two different forms of demanding visual tasks, MOT and VWM-cd. Collectively, these results reveal finer scale functional organization within the visually driven frontoparietal network.

4. Discussion

Visual attention and working memory tasks recruit a common set of frontoparietal regions that includes regions in lateral frontal cortex (LFC) and posterior parietal cortex (PPC). Here, we examined fine-scale

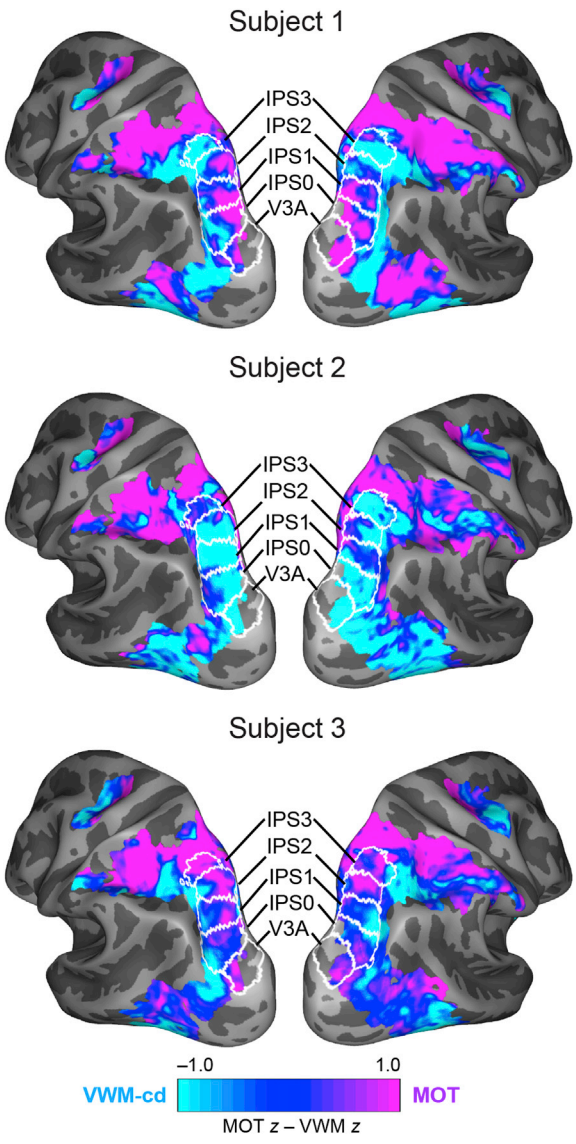

Fig. 5. Standardized comparison of MOT with VWM-cd task activation in three individual subjects.

functional organization of this network. Seed-to-vertex intrinsic functional connectivity analysis from LFC to PPC revealed two forms of group-level differences along the dorsomedial-ventrolateral and rostral-caudal axes. A functional connectivity gradient was observed along the dorsomedial to ventrolateral dimension: three distinct visual attention regions that span dorsomedial to ventrolateral LFC – superior precentral sulcus (sPCS), inferior precentral sulcus (iPCS), and mid inferior frontal sulcus (midIFS) – exhibit differential connectivity with corresponding dorsomedial-to-ventrolateral bands of PPC. Additionally, sPCS connectivity is relatively stronger to visual cortical area V3A, lateral occipital cortex, and to portions of the superior parietal lobule anterior to IPS3. This connectivity gradient in parietal cortex spatially coincides with a functional gradient for visuospatial attention processing: A multiple object tracking visual attention task (MOT) more strongly recruits the dorsomedial PPC region dominated by sPCS connectivity, whereas a visual working memory change detection task (VWM-cd) more strongly recruits the ventrolateral PPC region which exhibits stronger connectivity to iPCS and midIFS. Along the rostral-caudal axis, finer-scale differences in functional connectivity were observed. The relative connectivity strength of sPCS and iPCS seeds to PPC alternates along the rostral-caudal axis of intraparietal sulcus (IPS), with multiple peaks for each LFC seed. These differences mirror the pattern of visual field eccentricity representations observed across retinotopically mapped regions in the IPS. Peaks in sPCS connectivity to PPC coincide with regions that code peripheral visual field representations, whereas peaks in iPCS connectivity to PPC coincide with regions coding foveal visual field representations. Taken together, these results suggest that the visual frontoparietal cortical network is composed of fine-scale frontoparietal subnetworks that possess a high degree of functional specificity.

These findings extend prior research characterizing distributed functional networks in frontoparietal cortex. Extensive analyses of group-based functional connectivity suggest that these frontoparietal cortical attention regions, or the 'task positive system,' comprise multiple distributed networks (e.g., Yeo et al., 2011; Power et al., 2011; Doucet et al., 2011; Dixon et al., 2018), notably the dorsal attention (DAN) and cognitive control (CCN) networks, and putative CCN subnetworks. Recent studies investigating functional connectivity in individual subjects (Braga and Buckner, 2017; Gordon et al., 2017) have reported finer-scale functional networks between LFC and PPC, but significant differences across individuals have clouded the general interpretation of PPC functional organization. Consistent with these studies, the present findings reveal fine-grained functional distinctions within the visual frontoparietal regions by way of a dorsomedial-to-ventrolateral connectivity gradient. These results cannot merely be attributed to differential involvement of each frontal seed with either the canonical DAN or CCN. Both sPCS – often referred to as the human frontal eye fields (FEF) – and iPCS – sometimes called the inferior frontal junction – are putative LFC nodes of the DAN, while midIFS falls within the CCN (Yeo et al., 2011; Power et al., 2011; Doucet et al., 2011). However, all three nodes are co-activated by visual attention and WM and all three nodes show strong functional connectivity to both frontal and parietal nodes of the DAN, suggesting gradations in functional specificity rather than an all-or-none association with one large-scale network or another.

These resting-state connectivity differences correspond with task activation differences. Prior work examining an array of tasks (e.g., social, emotional, motor, WM) and rule manipulations have demonstrated a strong relationship between connectivity and task-evoked network structures at the level of the entire cerebral cortex (e.g., Cole et al., 2014). Here, at a finer scale, we observe a similarly tight link between intrinsic connectivity and functional organization. Our two tasks, a visual working memory change detection (VWM-cd) task and a visual attention multiple object tracking (MOT) task, share many common aspects of visual attentional processing. Both are attentionally demanding, and they may share additional processes, such as the filtering out of distracting information (e.g., Bettencourt et al., 2011). Nevertheless, the tasks differ in their fine-scale pattern of activation in PPC, and specific patterns of functional connectivity with 3 task-activated LFC regions capture these task differences. This difference in activation could reflect a difference between visual WM and visual attention processing, although a recent report suggests otherwise (Sheremata et al., 2018). Additional aspects differentiating the two tasks may be key factors. In contrast to the VWM-cd paradigm, the MOT paradigm requires that the subject dynamically update the spatial location of the target disks, thus raising the possibility that MOT task recruitment reflects the updating of a priority map – the representation of external stimuli or their locations according to their behavioral priority (Itti and Koch, 2000; Fecteau and Munoz, 2006; Bisley and Goldberg, 2010). Consistent with our findings in LFC, evidence suggests that sPCS, but not iPCS, acts as a priority map: for example, a classifier employed by Jerde et al. (2012) successfully predicted the location of interest (prioritized hemifield) in one dataset (attention, working memory, or intention) when trained on either of the other two datasets in sPCS, but not in iPCS. The VWM-cd paradigm, in contrast, requires that the subject store target feature information (orientation) over the course of a delay period. The observed differences between VWM-cd and MOT may thus represent a difference between WM retention and spatial updating of a priority map, respectively, or, more broadly, a difference between local and global attention. The precise

functional roles of these subnetworks remain unresolved and deserving of future exploration.

Along the rostral-caudal axis of IPS, the relative intrinsic functional connectivity strength of sPCS and iPCS alternates. Their peaks and troughs of relative functional connectivity occur near the areal boundaries in retinotopically defined IPS regions, rather than near the centers of the regions. iPCS connectivity dominates at the boundaries of IPS0/1 and IPS2/3 bilaterally, and this is more prevalent along the lateral portions of these borders; while sPCS connectivity dominates elsewhere within the retinotopic IPS regions. Visual field representations of the fovea lie on the lateral portions of IPS in two punctate regions, at the IPS0/1 border and at the IPS2/3 border (Swisher et al., 2007; Mackey et al., 2017). Each foveal representation forms the center of a visual field map cluster encompassing multiple cortical areas (Wandell et al., 2007; Mackey et al., 2017). These established foveal representations correspond with the regions where iPCS connectivity is strongest within retinotopic IPS. Conversely, the regions where sPCS connectivity dominates correspond with representations of the peripheral visual field. The observations that iPCS connectivity is stronger for representations of the central visual field and sPCS connectivity is stronger for representations of the peripheral visual field point to the intriguing notion that this connectivity pattern reflects differences between cognitive processes subserved by each subnetwork. The coding of fine scale visual features, which is essential to performance of the visual working memory change detection task, is most effectively performed by foveating those stimuli; therefore, there would be a clear functional utility in robust connections between frontal lobe iPCS, which is more strongly recruited for this task, and foveal representations within superior parietal lobule. Conversely, the coding and updating of the locations of covert visual spatial attention, which is essential to performance of the multiple object tracking task, requires processing of the peripheral visual field. sPCS corresponds to the FEF in humans which also plays a central role in guiding eye movements to peripheral targets (Hagler et al., 2007; Jerde et al., 2012; Szczepanski et al., 2010; Glasser et al., 2016; Tobyne et al., 2017). Therefore, robust connectivity between frontal sPCS and superior parietal lobule representations of the peripheral visual field offers clear utility for guiding eye movements and/or updating of covert spatial attention.

At present, studies mapping visual field coverage in sPCS and iPCS only show subtle or inconclusive evidence of visual field biases (e.g., Kastner et al., 2007; Mackey et al., 2017); thus, the precise retinotopic organization of these networks merits further study. Additionally, these findings suggest the possibility of predicting parietal retinotopic organization in individual subjects using resting-state functional connectivity. This adds to a growing body of work from our lab and others demonstrating the use of an individual's resting-state functional connectivity patterns – or connectivity fingerprint – to predict a variety of neural response patterns, such as DAN organization, visual and auditory attention, WM, social cognition, reward, motor action, and language (Jones et al., 2017; Osher et al., 2015, 2019; Saygin et al., 2012; Smittenaar et al., 2017; Tavor et al., 2016; Tobyne et al., 2018).

5. Conclusions

These findings provide evidence for the existence of a functional gradient within the visual frontoparietal cortical attentional network – a gradient with an organization more fine-grained than those of the canonical large-scale networks, and whose divisions seem to reflect both visual hemifield representation as well as aspects of visual working memory and attention. In an examination of cerebellar contributions to visual attention (Brissenden et al., 2018), we also observed similar functional gradients within PPC in the patterns of connectivity with sub-regions of cerebellar lobules VIIb/VIIIa. Many questions remain unresolved, such as the precise nature of these functional distinctions, the manner in which they interact with visual field representations, and whether similar networks appear across other sensory modalities. Future work should pursue these areas to progress our understanding of frontoparietal cortical circuitry and the roles of these networks in supporting cognitive processing.

Declaration of competing interest

The authors declare no competing financial interests.

CRediT authorship contribution statement

Ray W. Lefco: Investigation, Writing - original draft, Visualization. **James A. Brissenden:** Methodology, Software, Visualization, Writing - review & editing. **Abigail L. Noyce:** Resources, Data curation. **Sean M. Tobyne:** Methodology, Data curation. **David C. Somers:** Conceptualization, Writing - review & editing, Supervision.

Acknowledgements

This work was funded by National Institutes of Health grants R01-EY022229, NIH R21-EY027703 to D.C.S., F31-NS103306 to S.M.T., F31-MH101963 to S.W.M, F32-EY026796 to A.L.N., as well as National Science Foundation grants DGE-1247312 to J.A.B and BCS-1829394 to D.C.S. We thank Joseph McGuire and Sam Ling for their thoughtful comments on the manuscript. The views expressed in this article do not necessarily represent the views of the NIH, NSF, or the United States Government. The authors declare no competing financial interests.

Appendix A. Supplementary data

Supplementary data to this article can be found online at https://doi.org/10.1016/j.neuroimage.2020.117029.

References

Badre, D., Kayser, A.S., D'Esposito, M., 2010. Frontal cortex and the discovery of abstract action rules. Neuron 66, 315–326.
Barch, D.M., Burgess, G.C., Harms, M.P., Petersen, S.E., Schlaggar, B.L., Corbetta, M., Glasser, M.F., Curtiss, S., Dixit, S., Feldt, C., Nolan, D., Bryant, E., Hartley, T., Footer, O., Bjork, J.M., Poldrack, R., Smith, S., Johansen-Berg, H., Snyder, A.Z., Van Essen, D.C., WU-Minn HCP Consortium, 2013. Function in the human connectome: task-fMRI and individual differences in behavior. Neuroimage 80, 169–189.
Bates, D., Mächler, M., Bolker, B., Walker, S., 2015. Fitting linear mixed-effects models using lme4. J. Stat. Software 67.
Bettencourt, K.C., Xu, Y., 2016. Decoding the content of visual short-term memory under distraction in occipital and parietal areas. Nat. Neurosci. 19, 150–157.
Bettencourt, K.C., Michalka, S.W., Somers, D.C., 2011. Shared filtering processes link attentional and visual short-term memory capacity limits. J. Vis. 11, 22.
Bisley, J., Goldberg, M., 2010. Attention, intention, and priority in the parietal lobe. Annu. Rev. Neurosci. 33, 1–21.
Boynton, G.M., Engel, S.A., Glover, G.H., Heeger, D.J., 1996. Linear systems analysis of functional magnetic resonance imaging in human V1. J. Neurosci. 16, 4207–4221.
Braga, R.M., Buckner, R.L., 2017. Parallel interdigitated distributed networks within the individual estimated by intrinsic functional connectivity. Neuron 95, 457–471.
Brainard, D.H., 1997. The psychophysics toolbox. Spatial Vis. 10, 433–436.
Brissenden, J.A., Tobyne, S.M., Osher, D.E., Levin, E.J., Halko, M.A., Somers, D.C., 2018. Topographic cortico-cerebellar networks revealed by visual attention and working memory. Curr. Biol. 28, 3364–3372.
Brissenden, J.A., Levin, E.J., Osher, D.E., Halko, M.A., Somers, D.C., 2016. Functional evidence for a cerebellar node of the dorsal attention network. J. Neurosci. 36, 6083–6096.
Burgess, G., Kandala, S., Nolan, D., Laumann, T., Power, J., Adeyemo, B., Harms, M., Peterson, S., Barch, D., 2016. Evaluation of denoising strategies to address motion-correlated artifact in resting state fMRI data from the Human Connectome Project. Brain Connect. 6, 669–680.
Carp, J., 2013. Optimizing the order of operations for movement scrubbing: comment on Power et al. Neuroimage 76, 436–438.
Cole, M.W., Bassett, D.S., Power, J.D., Braver, T.S., Petersen, S.E., 2014. Intrinsic and task-evoked network architectures of the human brain. Neuron 83, 238–251.
Dale, A.M., Fischl, B., Sereno, M.I., 1999. Cortical surface-based analysis. I. Segmentation and surface reconstruction. Neuroimage 9, 179–894.
Desikan, R.S., Ségonne, F., Fischl, B., Quinn, B.T., Dickerson, B.C., Blacker, D., Buckner, R.L., Dale, A.M., Maguire, R.P., Hyman, B.T., Albert, M.S., Killiany, R.J., 2006. An automated labeling system for subdividing the human cerebral cortex on MRI scans into gyral based regions of interest. Neuroimage 31, 968–980.
Dixon, M.L., De La Vega, A., Mills, C., Andrews-Hanna, J., Spreng, R.N., Cole, M.W., Christoff, K., 2018. Heterogeneity within the frontoparietal control network and its

relationship to the default and dorsal attention networks. Proc. Natl. Acad. Sci. U.S.A. 115, E1598–E1607.
Doucet, G., Naveau, M., Petit, L., Delcroix, N., Jobard, G., Tzourio-Mazoyer, N., Mazoyer, B., Mellet, E., Joliot, M., 2011. Brain activity at rest: a multiscale hierarchical functional organization. J. Neurophysiol. 105, 2753–2763.
Eklund, A., Nichols, T.E., Knutsson, H., 2016. Cluster failure: why fMRI inferences for spatial extent have inflated false-positive rates. Proc. Natl. Acad. Sci. U.S.A. 113, 7900–7905.
Ester, E.F., Sutterer, D.W., Serences, J.T., Awh, E., 2016. Feature-selective attentional modulations in human frontoparietal cortex. J. Neurosci. 36, 8188–8199.
Fecteau, J., Munoz, D., 2006. Salience, relevance, and firing: a priority map for target selection. Trends Cognit. Sci. 10, 382–390.
Fischl, B., 2012. FreeSurfer. Neuroimage 62, 774–781.
Glasser, M.F., Coalson, T.S., Robinson, E.C., Hacker, C.D., Harwell, J., Yacoub, E., Ugurbil, K., Andersson, J., Beckmann, C.F., Jenkinson, M., Smith, S.M., Van Essen, D.C., 2016. A multi-modal parcellation of human cerebral cortex. Nature 536, 171–178.
Gordon, E.M., Laumann, T.O., Gilmore, A.W., Newbold, D.J., Greene, D.J., Berg, J.J., Ortega, M., Hoyt-Drazen, C., Gratton, C., Sun, H., Hampton, J.M., Coalson, R.S., Nguyen, A.L., McDermott, K.B., Shimony, J.S., Snyder, A.Z., Schlaggar, B.L., Petersen, S.E., Nelson, S.M., Dosenbach, N.U.F., 2017. Precision functional mapping of individual human brains. Neuron 95, 791–807.
Hagler, D.J., Riecke, L., Sereno, M.I., 2007. Parietal and superior frontal visuospatial maps activated by pointing and saccades. Neuroimage 35, 1562–1577.
Hagler Jr., D.J., Sereno, M.I., 2006. Spatial maps in frontal and prefrontal cortex. Neuroimage 29, 567–577.
Itti, L., Koch, C., 2000. A saliency-based search mechanism for overt and covert shifts of visual attention. Vis. Res. 40, 1489–1506.
Jerde, T.A., Merriam, E.P., Riggall, A.C., Hedges, J.H., Curtis, C.E., 2012. Prioritized maps of space in human frontoparietal cortex. J. Neurosci. 48, 17382–17390.
Jones, O.P., Voets, N.L., Adcock, J.E., Stacey, R., Jbabdi, S., 2017. Resting connectivity predicts task activation in pre-surgical populations. Neuroimage Clin. 13, 378–412.
Kastner, S., DeSimone, K., Konen, C.S., Szczepanski, S.M., Wiener, K.S., Schneider, Ka, 2007. Topographic maps in human frontal cortex revealed in memory-guided saccade and spatial working-memory tasks. J. Neurophysiol. 97, 3494–3507.
Konen, C.S., Kastner, S., 2008. Representation of eye movements and stimulus motion in topographically organized areas of human posterior parietal cortex. J. Neurosci. 28, 8361–8375.
Kuznetsova, A., Brockhoff, P.B., Christensen, R.H.B., 2017. lmerTest package: tests in linear mixed effects models. J. Stat. Software 82.
Lenth, R.V., 2016. Least-squares means: the R package lsmeans. J. Stat. Software 69.
Mackey, W.E., Winawer, J., Curtis, C.E., 2017. Visual field map clusters in human frontoparietal cortex. eLife 6, 1–23.
Mars, R.B., Jbabdi, S., Sallet, J., O'Reilly, J.X., Croxson, P.L., Olivier, E., Noonan, M.P., Bergmann, C., Mitchell, A.S., Baxter, M.G., Behrens, T.E.J., Johansen-Berg, H., Tomassini, V., Miller, K.L., Rushworth, M.F.S., 2011. Diffusion-weighted imaging tractography-based parcellation of the human parietal cortex and comparison with human and macaque resting-state functional connectivity. J. Neurosci. 31, 4087–4100.
Michalka, S.W., Kong, L., Rosen, M.L., Shinn-Cunningham, B.G., Somers, D.C., 2015. Short-term memory for space and time flexibly recruit complementary sensory-biased frontal lob attention networks. Neuron 87 (4), 882–892.
Nichols, T.E., Holmes, A.P., 2002. Nonparametric permutation tests for functional neuroimaging: a primer with examples. Hum. Brain Mapp. 15, 1–25.
Noyce, A.L., Tobyne, S.M., Michalka, S.W., Shinn-Cunningham, B., Somers, D.C., 2018. But wait, there's more! Six bilateral sensory-biased regions in human frontal cortex. J. Vis. 18 (10), 114.
Noyce, A.L., Cestero, N., Michalka, S.W., Shinn-Cunningham, B.G., Somers, D.C., 2017. Sensory-biased and multiple-demand processing in human lateral frontal cortex. J. Neurosci. 37, 8755–8766.
Osher, D.E., Brissenden, J.A., Somers, D.C., 2019. Predicting an individual's dorsal attention network activity from functional connectivity fingerprints. J. Neurophysiol. 122, 232–240.
Osher, D.E., Saxe, R.R., Koldewyn, K., Gabrieli, J.D.E., Kanwisher, N., Saygin, Z.M., 2015. Structural connectivity fingerprints predict cortical selectivity for multiple visual categories across cortex. Cerebr. Cortex 26, 1668–1683.
Pelli, D.G., 1997. The VideoToolbox software for visual psychophysics: transforming numbers into movies. Spatial Vis. 10, 437–442.
Power, J.D., Barnes, K.A., Snyder, A.Z., Schlaggar, B.L., Petersen, S.E., 2012. Spurious but systematic correlations in functional connectivity MRI networks arise from subject motion. Neuroimage 59, 2142–2154.
Power, J.D., Cohen, A.L., Nelson, S.M., Wig, G.S., Barnes, K.A., Church, J.A., Vogel, A.C., Laumann, T.O., Miezin, F.M., Schlaggar, B.L., Petersen, S.E., 2011. Functional network organization of the human brain. Neuron 72, 665–678.
Sallet, J., Mars, R.B., Noonan, M.P., Neubert, F.X., Jbabdi, S., O'Reilly, J.X., Filippini, N., Thomas, A.G., Rushworth, M.F., 2013. The organization of dorsal frontal cortex in humans and macaques. J. Neurosci. 33, 5108–5112.
Saygin, Z.M., Osher, D.E., Koldewyn, K., Reynolds, G., Gabrieli, J.D.E., Saxe, R.R., 2012. Anatomical connectivity patterns predict face selectivity in the fusiform gyrus. Nat. Neurosci. 15, 321–327.
Sereno, M.I., Pitzalis, S., Martinez, A., 2001. Mapping of contralateral space in retinotopic coordinates by a parietal cortical area in humans. Science 294, 1350–1354.
Setsompop, K., Gagoski, B.A., Polimeni, J.R., Witzel, T., Wedeen, V.J., Wald, L.L., 2012. Blipped-controlled aliasing in parallel imaging for simultaneous multislice echo planar imaging with reduced g-factor penalty. Magn. Reson. Med. 67, 1210–1224.
Sheremata, S.L., Somers, D.C., Shomstein, S., 2018. Visual short-term memory activity in parietal lobe reflects cognitive processes beyond attentional selection. J. Neurosci. 38, 1511–1519.
Sheremata, S.L., Bettencourt, K.C., Somers, D.C., 2010. Hemispheric asymmetry in visuotopic posterior parietal cortex emerges with visual short-term memory load. J. Neurosci. 30, 12581–12588.
Silver, M.A., Ress, D., Heeger, D.J., 2005. Topographic maps of visual spatial attention in human parietal cortex. J. Neurophysiol. 94, 1358–1371.
Smith, S.M., Nichols, T.E., 2009. Threshold-free cluster enhance- ment: addressing problems of smoothing, threshold dependence and localisation in cluster inference. Neuroimage 44, 83–98.
Smittenaar, P., Kurth-Nelson, Z., Mohammadi, S., Weiskopf, N., Dolan, R.J., 2017. Local striatal reward signals can be predicted from corticostriatal connectivity. Neuroimage 159, 9–17.
Straw, A.D., 2008. Vision egg: an open-source library for realtime visual stimulus generation. Front. Neuroinf. 2, 4.
Swisher, J.D., Halko, M.A., Merabet, L.B., McMains, S.A., Somers, D.C., 2007. Visual topography of human intraparietal sulcus. J. Neurosci. 27, 5326–5337.
Szczepanski, S.M., Konen, C.S., Kastner, S., 2010. Mechanisms of spatial attention control in frontal and parietal cortex. J. Neurosci. 30, 148–160.
Tavor, I., Jones, O.P., Mars, R.B., Smith, S.M., Behrens, T.E., Jbabdi, S., 2016. Task-free MRI predicts individual differences in brain activity during task performance. Science 352, 216–220.
Tobyne, S.M., Osher, D.E., Michalka, S.W., Somers, D.C., 2017. Sensory-biased attention networks in human lateral frontal cortex revealed by intrinsic functional connectivity. Neuroimage 162, 362–372.
Tobyne, S.M., Somers, D.C., Brissenden, J.A., Michalka, S.W., Noyce, A.L., Osher, D.E., 2018. Prediction of individualized task activation in sensory modality-selective frontal cortex with 'connectome fingerprinting. Neuroimage 183, 173–185.
Wang, L., Mruczek, R.E.B., Arcaro, M.J., Kastner, S., 2015. Probabilistic maps of visual topography in human cortex. Cerebr. Cortex 25, 3911–3931.
Yeo, B.T.T., Krienen, F.M., Sepulcre, J., Sabuncu, M.R., Lashkari, D., Hollinshead, M., Roffman, J.L., Smoller, J.W., Zöllei, L., Polimeni, J.R., Fischl, B., Liu, H., Buckner, R.L., 2011. The organization of the human cerebral cortex estimated by intrinsic functional connectivity. J. Neurophysiol. 106, 1125–1165.